

EFFECTIVE MODELS FOR CO₂ MIGRATION IN GEOLOGICAL SYSTEMS WITH VARYING TOPOGRAPHY

Sarah E. Gasda*, Halvor M. Nilsen[†] and Helge K. Dahle[‡]

*Center for Integrated Petroleum Research, Uni Research
Allégaten 41, 5020 Bergen, Norway
e-mail: sarah.gasda@uni.no, web page: <http://cipr.uni.no/>

[†]Applied Mathematics, SINTEF
Forskningsveien 1, 0314 Oslo, Norway

[‡]Department of Mathematics, University of Bergen
Johannes Brunsgate 12, 5020 Bergen, Norway

Key words: Geological CO₂ sequestration, vertical equilibrium, caprock roughness, up-scaled models, capillary fringe

1 INTRODUCTION

Geological CO₂ sequestration relies on a competent sealing layer, or caprock, that bounds the formation top and prevents vertical migration of fluids^{1,2}. Modeling studies have shown that the caprock boundary can significantly decrease updip migration speed of CO₂ and increase structural trapping³. The trapping phenomenon depends on the structure and topography, or roughness, of the caprock that can be characterized at different spatial scales. For instance, regional-scale features such as domes, traps, and spill points can be detected in seismic surveys⁴ and have been shown to affect large-scale migration patterns². However, subscale structural and topographical variability, known as rugosity, exists below seismic detection limits but can be measured at the scale of centimeters and meters using LiDAR scanning of formation outcrops⁵⁻⁷. Less is known about the actual impact of subscale structural rugosity on CO₂ plume migration.

Practically speaking, given the large scales required to model commercial scale CO₂ storage projects and the limitations on computational power⁸, only regional scale caprock topography can be resolved using standard discretization techniques. The well-known vertical equilibrium (VE) model, which allows for partial integration of the multiphase flow equations^{3,8,9}, captures CO₂ migration along variable caprock topography more reliably and efficiently compared to a standard full-dimensional simulator for systems in which the assumptions of vertical equilibrium and gravity segregation are valid. Therefore, caprock variability that exists below the scale of VE model resolution must be handled by up-scaling. In this paper, we summarize the derivation of effective equations for fine-scale

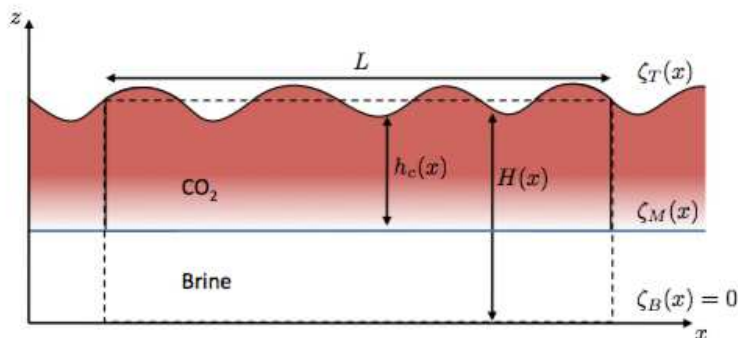


Figure 1: Fine-scale caprock topography having spatially varying thickness $H(x)$ and CO_2 thickness $h_c(x)$ within the averaging length L . The system has a flat bottom $\zeta_B = 0$ and flat CO_2 -brine interface.

variability in caprock topography using steady state homogenization^{10,11} adapted for the VE modeling framework. We build upon previous work based on a sharp interface assumption¹² by including a capillary fringe in the derivation of the effective equations. Herein, we investigate the relative importance of subscale rugosity on CO_2 plume migration and immobilization compared to other subscale processes that occur in large-scale systems.

2 MODEL APPROACH

Our objective is to derive an effective model for the system depicted in Figure 1 that consists of a reservoir with top and bottom boundaries whose vertical locations are described by functions $\zeta_T(x, y)$ and $\zeta_B(x, y)$, respectively. Within this aquifer, two mobile fluid phases exist, CO_2 and brine, along with associated residual phases. We assume that the fluid phases are in gravity-capillary equilibrium. The vertical fluid pressure is also at equilibrium, which implies that at any given horizontal location, the fluid phases are vertically distributed according to density and the vertical flow component for each phase is negligible.

2.1 VE Model

We horizontally average the VE equations for an aquifer with significant caprock roughness, i.e. a varying top boundary. The VE model equations are formulated by vertical integration of 3D flow equations. The resulting 2D horizontal flow equations consist of depth-integrated quantities such as saturation, phase fluxes, permeability and relative permeability. Here, horizontal flow implies parallel to predominant flow direction. The resulting VE model equations^{3,13} are,

$$\frac{\partial}{\partial t} (H\Phi S_\alpha) + \nabla_{\parallel} \cdot \mathbf{F}_{\parallel\alpha} = Q_\alpha, \quad \alpha = c, b. \quad (1)$$

In the integrated equation, Φ is depth-averaged porosity, S_α is the depth-integrated saturation, H is spatially varying aquifer thickness, defined as $H(x, y) = \zeta_T(x, y) - \zeta_B(x, y)$, Q_α is the depth-integrated source/sink term, and $(\cdot)_\parallel$ represent lateral operators and quantities. Depth-integrated saturation is defined as

$$H\Phi S_\alpha = \int_{\zeta_B}^{\zeta_T} \phi s_\alpha dz, \quad \alpha = c, b. \quad (2)$$

The mass fluxes $\mathbf{F}_{\parallel\alpha}$ are obtained by vertically integrating the lateral component of phase fluxes and gives the resulting upscaled flux expressions,

$$\mathbf{F}_b = -\frac{H\mathbf{K}_{\parallel b} \cdot \mathbf{K}_\parallel}{\mu_b} \cdot [\nabla P_b - \nabla(\mathbf{e}_3 \cdot \mathbf{g}\rho_b\zeta_B) - \rho_b\mathbf{g}], \quad (3)$$

$$\mathbf{F}_c = -\frac{H\mathbf{K}_{\parallel c} \cdot \mathbf{K}_\parallel}{\mu_c} \cdot [\nabla P_c + \nabla(\mathbf{e}_3 \cdot \mathbf{g}\Delta\rho\zeta_M) - \nabla(\mathbf{e}_3 \cdot \mathbf{g}\rho_b\zeta_B) - \rho_c\mathbf{g}], \quad (4)$$

where $\Delta\rho = \rho_b - \rho_c$. The depth-integrated permeability and relative permeability tensors are defined as,

$$H\mathbf{K}_\parallel = \int_{\zeta_B}^{\zeta_T} \mathbf{k}_\parallel dz, \quad H\mathbf{K}_{\parallel\alpha} \cdot \mathbf{K}_\parallel = \int_{\zeta_B}^{\zeta_T} \mathbf{k}_\parallel k_\alpha dz, \quad \alpha = c, b. \quad (5)$$

For convenience, we will omit the $(\cdot)_\parallel$ notation from this point forward. Together, Eqns (1)–(5) represent the fine-scale system of equations.

The above equations may be solved with a capillary fringe, which creates a transition zone of saturation above the ζ_M interface where both fluids are mobile¹⁴. Under the assumption of a gravity-capillary equilibrium, the vertical distribution in saturation can be determined by inverting the local capillary pressure-saturation function. From this, the vertical distribution of relative permeability $k_\alpha(z)$ is known *a priori* and can be integrated in Eqn (5) to obtain $\mathbf{K}_{\parallel\alpha}$ for each phase.

2.2 Upscaled Model

The VE equations are integrated horizontally to obtain effective medium functions for a rough caprock system. In doing so, we follow traditional homogenization techniques that have been developed for upscaling permeability and relative permeability of heterogeneous media, where the heterogeneity is in local permeability. We adapt this steady-state homogeneous equation approach to a vertically integrated system in which the heterogeneity is aquifer thickness. The end result is a set of effective permeability and relative permeability functions that capture both the migration retardation and enhanced trapping of CO₂ due to subscale topographical features as well as the impact of a capillary fringe on large-scale fluid flow.

We derive the effective functions analytically for a vertical cross-section (x - z) of an aquifer (Figure 1). This system has a flat bottom $\zeta_B(x) = 0$, and gravity is neglected.

The objective of upscaling is to replace the varying top boundary with a flat surface. This results in an aquifer height that is constant and equal to the average of the fine-scale thickness over the averaging length,

$$\bar{H} = \frac{1}{L} \int_0^L [\zeta_T(x) - \zeta_B(x)] dx. \quad (6)$$

The basic approach is to posit a homogeneous equation at the average scale composed of horizontally averaged quantities. If we assume steady-state flow over the averaging length then the fine-scale single-phase flow equation can be integrated and set equal to the homogeneous equation,

$$F_x = \frac{1}{L} \int_0^L \left(-\frac{HK}{\mu} \frac{dP}{dx} \right) dx = -\frac{\bar{H}\bar{K}}{\mu} \frac{\Delta P}{\Delta L}, \quad (7)$$

from which we obtain,

$$\frac{1}{\bar{H}\bar{K}} = \frac{1}{L} \int_0^L \frac{1}{HK} dx. \quad (8)$$

Eqn (8) indicates that the effective transmissibility ($\bar{H}\bar{K}$) for an aquifer of varying thickness is the harmonic average of fine-scale transmissibility over the length scale of interest.

For relative permeability, additional assumptions are required regarding the fine-scale saturation. Our approach is based on the capillary equilibrium assumption^{10,11} that is adapted to the VE rough caprock system and becomes an assumption on the CO₂-brine interface. For small pressure gradients and a horizontal averaging length much smaller than the domain, the ζ_M interface is essentially flat. This means that $\nabla\zeta_M = 0$ in Eqns (3) and (4), and the fine-scale saturations can be fixed during the averaging step. Then in a similar manner shown in Eqn (7), the two-phase steady-state flow equation is compared with the corresponding homogeneous equation, which results in upscaled relative permeability of the form,

$$\frac{1}{\bar{H}\bar{K}\bar{K}_\alpha} = \frac{1}{L} \int_0^L \frac{1}{h_\alpha K K_\alpha} dx. \quad (9)$$

We observe that the effective relative permeability is a harmonic mean of fine-scale relative permeability values weighted by the corresponding transmissibility. For CO₂, this implies that if $h_c(x) = 0$ at any point within the averaging window then $\bar{K}_c = 0$. Therefore, CO₂ has zero mobility for locations of the CO₂ interface equal to or higher than the local minimum of the topography.

Numerical homogenization can be performed by simulating steady-state flow at the fine-scale with the non-upscaled VE model. The average flux can be calculated and used to determine the effective permeability and relative permeability from the homogeneous equations. For 2D caprock surfaces, numerical homogenization is almost always necessary.

3 MODEL APPLICATION

The effective model is applied to an aquifer cross-section with idealized topography. The homogeneous aquifer has a top surface $\zeta_T(x)$ is described by a sinusoidal function,

$$\zeta_T(x) = \bar{H} (1 + a \sin \omega x), \quad \zeta_B(x) = 0, \quad (10)$$

with scaled amplitude $a = A/\bar{H} = 0.1$, wavelength $\omega = 0.01\pi$, and average aquifer thickness $\bar{H} = 100$ m. The aquifer has homogeneous permeability k and porosity ϕ and a 1% tilt. The boundary conditions, fluid and rock properties can be found elsewhere¹².

Reference simulations were performed using the VE model, resolving the caprock topography with a relatively fine grid. One simulation assumed a sharp interface at the ζ_M interface and the second included a capillary fringe. The local relative permeability function and local capillary pressure-saturation model are simple power laws,

$$k_b = s_{b,n}^3, \quad k_c = k_c^r (1 - s_{b,n})^3, \quad P_c = P_0 (s_{b,n})^{-1/2}, \quad (11)$$

where $k_c^r = 0.5265$ is the CO₂ endpoint relative permeability, and $s_{b,n}$ is the apparent brine saturation computed with residual brine and CO₂ saturations set to $s_{b,r} = 0.1$ and $s_{c,r} = 0.2$, respectively. The capillary pressure parameter $P_0 = 0.2$ bar, or 2×10^4 Pa. For the sharp-interface case $P_0 = 0$.

In the sharp-interface case (SI), the effective permeability (Eqn (8)) and relative permeability functions (Eqn (9)) can be computed analytically for this system,

$$\bar{K} = k \sqrt{(1 - a^2)}, \quad \bar{K}_c = k_c^r \frac{\sqrt{(\bar{h}_c/\bar{H})^2 - a^2}}{\sqrt{1 - a^2}}, \quad \bar{K}_b = \frac{\bar{h}_b}{\bar{H}}. \quad (12)$$

For the case of capillary fringe (CF), the integration can be performed numerically.

The impact of capillary pressure on relative permeability is apparent in the convex curvature of the flat caprock ($a=0$) functions near endpoint saturations (Figure 2b), compared with linear functions in the SI case in Figure 2a. When roughness is included, the same general curvature is maintained in the CF case, while the SI case becomes non-linear at low CO₂ saturations but increases sharply. Both roughness curves meet the flat caprock curve quite rapidly, which implies that caprock roughness is a local effect that only impacts relative permeability for relatively thin CO₂ plumes while the capillary fringe is a global effect that persists for all saturation values. We also observe that the effective CO₂ functions result in a “residual” CO₂ saturation, where CO₂ is structurally trapped until the ζ_M interface has moved below the local minimum of the local topography. the effect is smaller for the CF than the SI case because the capillary transition zone spreads CO₂ vertically and reduces depth-averaged saturation for the same ζ_M interface location.

The effective model compares well with the resolved simulations in both the sharp-interface and capillary fringe cases. The effective simulations slightly underestimate the tip speed, which is due to neglecting gravity during the averaging step that leads to

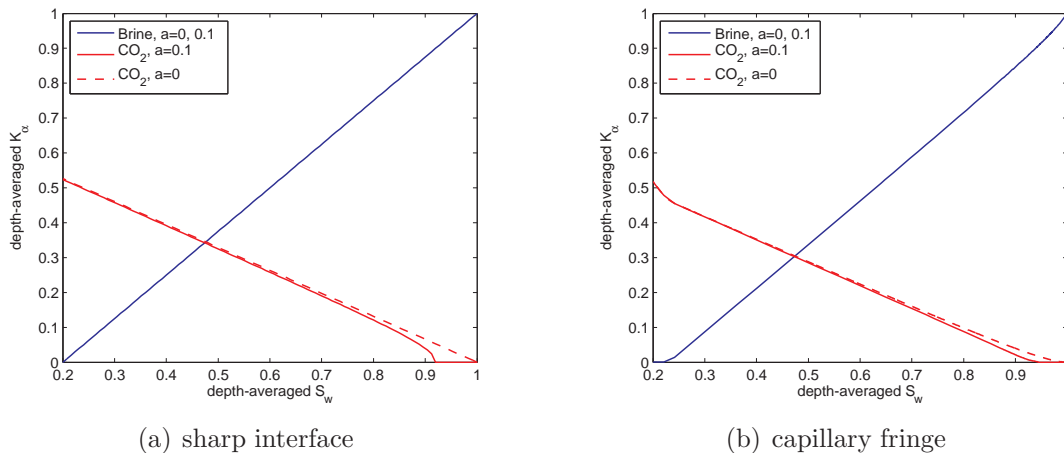


Figure 2: Upscaled relative permeability functions for a caprock surface $\zeta_T(x) = \bar{H}(1 + a \sin x)$ assuming a sharp interface (a) and a capillary fringe (b). CO₂ curves are shown for $a = 0.1$ and $a = 0$.

an overestimation of structurally trapped CO₂. We observe that the maximum upslope plume extent (Figure 4) is significantly impacted by a rough caprock compared with a flat caprock ($a = 0$) in both cases. The plume speed reduction from a flat caprock is greater for a sharp interface than a capillary fringe. However, the strength of the capillary fringe depends on the characteristic length scale of the capillary transition zone ϵ^{14} compared with the amplitude of the roughness a . We introduce a dimensionless grouping,

$$\ell_{cr} = \frac{\epsilon}{A} = \frac{p_c^*}{a\bar{H}\Delta\rho g}, \quad (13)$$

where p_c^* is a characteristic variation of the local capillary pressure curve. For values of $\ell_{cr} \ll 1$, the rough caprock effect dominates while capillary effects are minimal. Conversely, when $\ell_{cr} \gg 1$, the capillary fringe has a greater impact on plume migration speed despite the structurally heterogeneous system.

4 SUMMARY AND CONCLUSIONS

Effective models are needed to describe CO₂ migration in structural heterogeneity that exists below the model resolution scale. A new model has been derived here using steady-state homogenization upscaling applied to the VE model equations under a range of capillary pressure conditions. This model gives a direction for modeling real systems by demonstrating that subscale heterogeneity can be captured by upscaling techniques. We also identify the scale that caprock roughness and rugosity becomes important compared to the capillary fringe. If the characteristic length of the capillary transition zone is much larger than the dominant amplitude of the structural heterogeneity that is difficult or impossible to resolve then the caprock roughness can be ignored. Otherwise, subscale rugosity must be modeled with upscaled functions or resolved by other means.

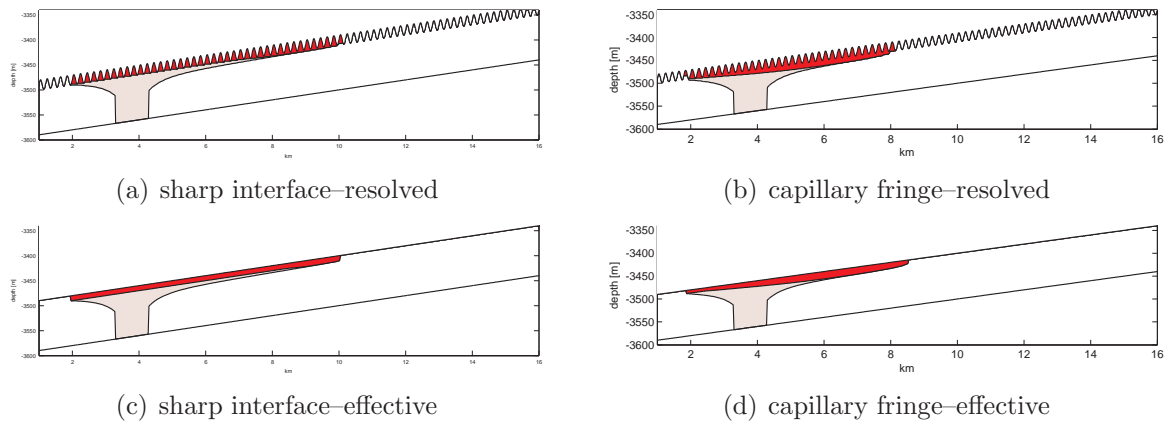


Figure 3: Resolved and effective model results for CO₂ plume (dark) and residual trapping (light).

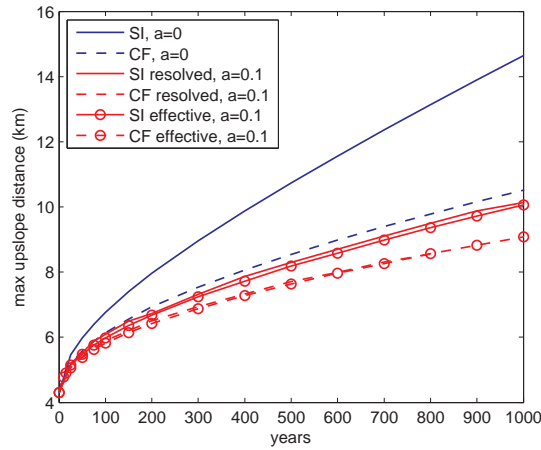


Figure 4: Maximum upslope extent of CO₂ over time for resolved and SI and CF effective simulations.

Acknowledgements. This work is funded under the MatMoRA-II project, which is financed by the Norwegian Research Council and Statoil.

References

- [1] Ambrose, W. A., Lakshminarasimhan, S., Holtz, M. H., Nunez-Lopez, V., Hovorka, S. D., and Duncan, I. Geologic factors controlling CO₂ storage capacity and permanence: case studies based on experience with heterogeneity in oil and gas reservoirs applied to CO₂ storage. *Environ. Geol.* **54**(8), 1619–1633 (2008).
- [2] Hermanrud, C., Andresen, T., Eiken, O., Hansen, H., Janbu, A., Lippard, J., Bolås, H. N., Simmenes, T. H., Teige, G. M. G., and Østmo, S. Storage of CO₂ in saline

- aquifers-lessons learned from 10 years of injection into the Utsira Formation in the Sleipner area. *Energy Procedia* **1**(1), 1997–2004 (2009).
- [3] Gray, W. G., Herrera, P., Gasda, S. E., and Dahle, H. K. Derivation of vertical equilibrium models for CO₂ migration from pore scale equations. *Int. J. Numer. Anal. Model.* (2011). in press.
- [4] Jackson, C. A.-L., Grunhagen, H., Howell, J. A., Larsen, A. L., Andersson, A., Boen, F., and Groth, A. 3d seismic imaging of lower delta-plain beach ridges: lower Brent Group, northern North Sea. *J. Geol. Soc. London* **167**, 1225–1236 (2010).
- [5] Pringle, J. K., Brunt, R. L., Hodgson, D. M., and Flint, S. S. Capturing stratigraphic and sedimentological complexity from submarine channel complex outcrops to digital 3D models, Karoo Basin, South Africa. *Petroleum Geoscience* **16**(4), 307–330 (2010).
- [6] Jones, R. R., McCaffrey, K. J. W., Clegg, P., Wilson, R. W., Holliman, N. S., Holdsworth, R. E., Imber, J., and Waggott, S. Integration of regional to outcrop digital data: 3D visualisation of multi-scale geological models. *Comput. Geosci.* **35**(1), 4–18 (2009).
- [7] Bellian, J., Kerans, C., and Jennette, D. Digital outcrop models: Applications of terrestrial scanning lidar technology in stratigraphic modeling. *J. Sediment. Res.* **75**(2), 166–176 (2005).
- [8] Nordbotten, J. M. and Celia, M. A. *Geological Storage of CO₂: Modeling Approaches for Large-Scale Simulation*. John Wiley & Sons, Inc., (2012).
- [9] Gasda, S. E., Nordbotten, J. M., and Celia, M. A. Vertical equilibrium with sub-scale analytical methods for geological CO₂ sequestration. *Computat. Geosci.* **13**(4), 469–481 (2009).
- [10] Pickup, G. and Stephen, K. An assessment of steady-state scale-up for small-scale geological models. *Petrol. Geosci.* **6**(3), 203–210 (2000).
- [11] Neuweiler, I. and Vogel, H.-J. Upscaling for unsaturated flow for non-Gaussian heterogeneous porous media. *Water Resour. Res.* **43**(3), W03443 (2007).
- [12] Gasda, S. E., Nilsen, H., Dahle, H., and Gray, W. Effective models for CO₂ migration in geological systems with varying topography. *Water Resour. Res.* (2012). under review.
- [13] Gasda, S. E., Nordbotten, J. M., and Celia, M. A. Vertically-averaged approaches for CO₂ injection with solubility trapping. *Water Resour. Res.* **47**, W05528 (2011).
- [14] Nordbotten, J. M. and Dahle, H. K. Impact of the capillary fringe in vertically integrated models for CO₂ storage. *Water Resour. Res.* **47**, W02537 (2011).